Optimizing the efficiency of triboelectric nanogenerators by surface nanoarchitectonics of graphene-based electrodes: A review

Journal Pre-proof

Optimizing the efficiency of triboelectric nanogenerators by surface nanoarchitectonics of graphene-based electrodes: A review

Deepak Deepak, Navneet Soin, Susanta Sinha Roy

PII: S2352-4928(23)00102-2

DOI: https://doi.org/10.1016/j.mtcomm.2023.105412

Reference: MTCOMM105412

To appear in: *Materials Today Communications*

Received date: 11 January 2023
Accepted date: 13 January 2023

Please cite this article as: Deepak Deepak, Navneet Soin and Susanta Sinha Roy, Optimizing the efficiency of triboelectric nanogenerators by surface nanoarchitectonics of graphene-based electrodes: A review, *Materials Today Communications,* (2023) doi:https://doi.org/10.1016/j.mtcomm.2023.105412

Optimizing the efficiency of triboelectric nanogenerators by surface nanoarchitectonics of graphene-based electrodes: A review

Deepak Deepak[a], Navneet Soin[b], Susanta Sinha Roy[a*]

[a] *Department of Physics, School of Natural Sciences, Shiv Nadar Institution of Eminence (SNIoE), NH-91, Greater Noida, Uttar Pradesh, 201314, India*

[b]*School of Engineering, Ulster University, Newtownabbey, Belfast, BT37 0QB, Northern Ireland, United Kingdom*

Abstract:

Since the discovery of triboelectric nanogenerators (TENGs), a significant body of research work has been undertaken for the modification of material properties to enhance their efficiency. These efforts have focused on judicious materials choice (large differences in work functions), enhanced charge-exchange density *via* hybridization (plasmonic, photo-enhancement, piezoelectric effect), enhanced contact area *via* nanostructuring and new device architectures. Whilst these efforts have led to a significant increase in the power density, but the rudimentary choice of metal electrode selection and subsequent charge transfer mechanism still demand attention. As such, low-dimensional carbon nanomaterials and in particular, graphene and its derivatives have been explored in the literature to overcome some of the drawbacks of the conventional metallic electrodes including fatigue and corrosion, especially in high humidity environments. Graphene with its exceptionally high surface area, high electrical conductivity and flexibility make itself an excellent material for enabling wearable electronics. In this review, we discuss the impact of graphene, graphene-based composite electrodes, doped graphene electrodes and laser-induced graphene (LIG) electrodes to improve the performance of TENGs. Also, the basic mechanism of charge transfer between different electrodes of the TENG device has been explained. Among all

graphene-based electrodes for TENG, laser-induced graphene electrodes show excellent performance owing to output power density 240 times higher than that of pristine graphene and 120 times more than graphene-based composite electrodes. Such use of functionalized graphene electrodes establishes the new steps towards the realization of flexible and transparent triboelectric nanogenerators.

Graphical abstract

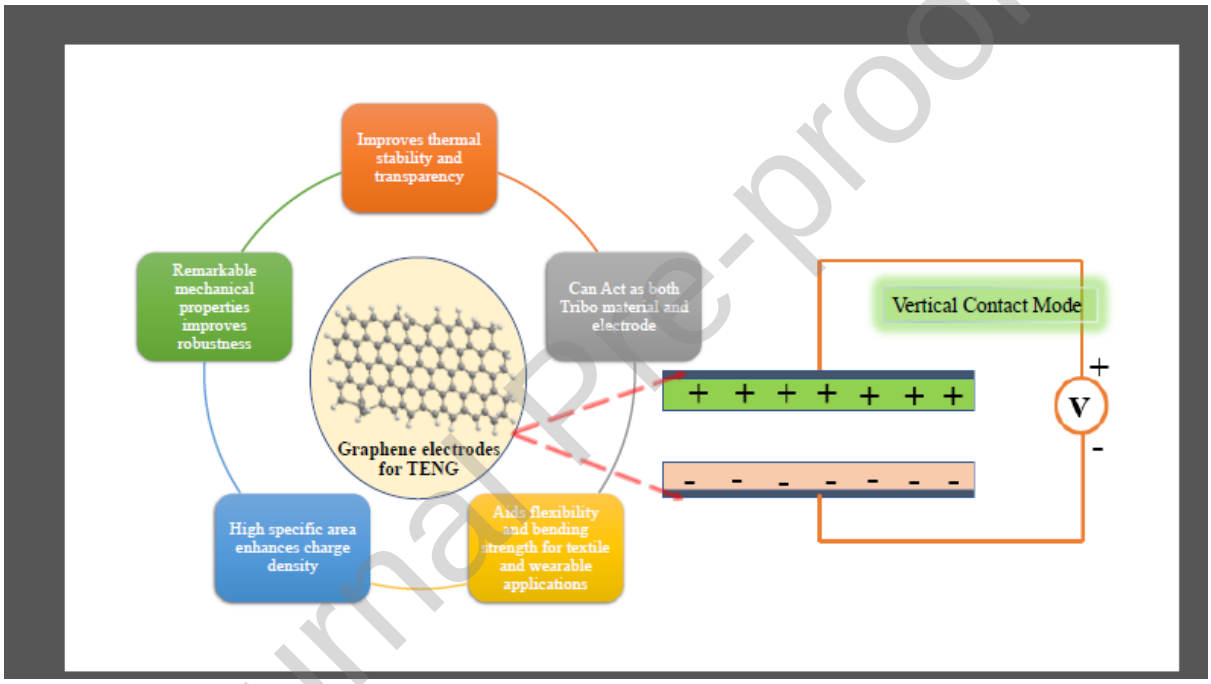

Keywords:

Graphene electrodes, Triboelectric nanogenerators, Laser-Induced graphene

1. Introduction

In the era of the Internet of Things, traditional energy and power sources are in high demand for the sustainable growth of the modern world. So, there has been a rapid rise in manufacturing of smart electronic systems which are wearable, lightweight, cost-effective and consume less power. Among all, wearable electronics have gained significant attention at

present due to their pervasive assets like portability, stretchability, biocompatibility and mainly routine life uses [1–3]. However, such electronic systems face limited power supplies from conventional batteries, which have an inadequate lifetime, and require frequent charging and/or replacement [4–6]. Moreover, batteries are built with toxic and hazardous chemicals which in turn can be a real risk to the environment [7,8]. With a rising population and limited resources, high power consumption can be a real peril for human civilization. To subdue this issue, the evolution of such systems is necessary which can drive energy from renewable sources like wind, solar, water and ambient surroundings [9]. Various types of energy forms like mechanical, solar and thermal etc. are being wasted every day, utilization of which can be an alternative to conventional power sources [10,11]. Amidst all forms of energy, mechanical energy is the most ubiquitous which can be found on a wide scale in the environment [12–15]. Harvesting mechanical energy from surroundings certainly leads to the evolution of self-powered sensors which can overcome the traditional power sources. In this regard, Z.L Wang and his group invented a series of energy harvesters like piezoelectric, thermoelectric and triboelectric nanogenerators[16,17]. Triboelectric nanogenerators (TENGs) show tremendous potential among all due to their exceptional ability to harvest energy at low frequency stage which quite unlikely to appear for both piezoelectric and thermoelectric[18,19]. Moreover, diverse material selectivity and inimitable ability of becoming self-powered sensors categorize TENGs into a special class of nanogenerators.

1.1 Basic mechanism and models of TENG

Triboelectric nanogenerators mainly consists of two materials of different electron affinity or work function with conductive electrode attached back through a circuit as shown in schematic diagram (figure 1). TENGs are based on a unique mechanism of contact electrification and electrostatic induction of two materials[20–22]. Contact electrification refers to the electrical charging of two materials when they get in physical contact with each

other due to different electron affinity. This electrical charging sets up a potential difference between two materials (fig1) during contact and when they moved away from each other, electrical equilibrium is disturbed, as a result charge flows through the circuit resulting in production of electrical energy [23,24]. Function of conducting electrodes is to set up a charge(Q) flow through external circuit [25] and the net electric potential difference between two electrodes $V_{oc}(x)$ can be defined as

$$\mathbf{V_{oc}(x) = - \frac{1}{C(x)} Q + V_{oc}(x)}$$

where x is the distance between two tribomaterials.

1.2 Charge transfer mechanism during contact electrification

Charge transfer mechanism during the contact of two tribo-materials is yet to be explored significantly. However, an electron cloud potential well model proposed by Cheng Xu et.al. [26] anticipates well for the charge transfer between two materials of different electron affinity. Electrons which are structurally localized within the molecular orbitals of certain atoms generate electron clouds. An atom can be considered as a potential well with valence electrons forming electron clouds. Schematic diagram of such movement of electrons is shown in figure 2. E_A and E_B are the energies of the highest occupied level and E_1 and E_2 are the threshold energy required for electrons to escape from the respective parent atom. Initially when there is no contact between two materials, there is no mutual movement of electrons due to trapping inside potential well. [fig 2a]. Once the two materials come in contact with each other there will be transfer of electrons from A to B [fig 2b] as a result of overlapping of electron clouds. After the separation of respective materials [2c] some electrons remain trapped inside material B due to the presence of energy barrier E_2. An elevation in temperature causes rapid energy fluctuations which in turn forces electrons to jump from

material B to material A [fig 2d] to regain original configuration. This method was applied and experimentally verified for the CE mechanism in TENG device demonstrated by Xu *et.al* [26]

1.3 Working Modes of TENG

Depending upon the electrode design and movement of triboelectric materials, TENGs can be classified into four different working modes [27], (a) Vertical contact separation mode, (b) Lateral sliding mode, (c) Single electrode mode and (d) Freestanding triboelectric layer mode.

(a) Vertical contact separation mode:

This mode entails two metal electrodes attached on the back of the two triboelectric materials namely, tribopositive and tribonegative. When mechanical force is applied on this setup, due to contact electrification, opposite charge develops on two materials and when the contact disappears, charge flows back through the electrode to balance the electrostatic equilibrium, resulting in output current [28] (figure3a). Charge flow originates an induced charged density σ') which can be written as

$$\boldsymbol{\sigma}' = \frac{\sigma d' \varepsilon_{r1}\varepsilon_{r2}}{d_1\varepsilon_{r1} + d'\varepsilon_{r1}\varepsilon_{r2} + d_2\varepsilon_{r2}}$$

Where d', ε_{r1} and ε_{r2} are the distance between two tribomaterials and relative permittivity of both triboelectric materials respectively and d_1 and d_2 are the thickness of these layers.

(b) Lateral Sliding mode

The fundamental structure of this mode is same as vertical contact mode with a difference in the movement of two tribo materials over each other. Lateral sliding of top layer over bottom

layer results in opposite charge generation due to their different electronegativity (figure3b). At complete separation, potential difference is setup between two electrodes and when the configuration is reversed, charge will flow back through electrodes to maintain the equilibrium resulting in current generation [29,30].

(c) Single electrode mode

This mode consists only top material and one electrode which is connected to ground (figure 3c). During the contact, these two-material become oppositely charged due to triboelectric effect. Throughout the motion of approaching and departing between two, local electric field is disturbed, as a result charge flows back to ground to maintain electrostatic equilibrium which in turn generates current [31,32] . Moreover, in single and lateral sliding mode, the electrode does not undergo significant cycling which is usually the case for the vertical contact separation and hence the mechanical property requirements are not that stringent.

(d) Freestanding triboelectric layer mode

This mode consists of only one triboelectric material sliding over two conducting electrodes (figure 3d). During the motion of triboelectric material over two electrodes, they get oppositely charged. A potential difference is setup during the back-and-forth motion of top layer over electrodes which is further responsible for current production [33].

Although TENGs are excellent alternative for some electronic systems but it has several drawbacks like low durability, high output impedance and deficiency of on demand output power supply [34]. Performance of TENGs depends on several aspects like charge density, judicious choice of tribo materials and surface morphology [35,36]. Surface charge density is quadratically related to output power density and hence prominently dominates the overall efficiency of TENGs [37,38]. However, circuit design, material surface modifications via

doping of the charge layer, electrode selection, and various electronic properties like conductivity and work function plays a vital role in boosting up the surface charge density [37].

Most of the practical applications of TENG require flexibility, stretchability, and deformity to harvest the mechanical energy from the arbitrary surface and routine life human movement [39]. Moreover, flexible self-powered sensors are useful in monitoring the real-time motional movement, human health, and energy from harsh environments [40,41]. So prudent selection of electrodes not only facilitates charge density but also fulfill the requirement of flexible devices [42]. To date, many conductive materials have been used as a back electrode in TENGs including metals, carbon-based materials, polymers etc. Conventional metallic electrodes indubitably enhance the conductivity and ease the electron flow, but their stiffness and rigidity make them inferior nominee in race of designing flexible TENGs [43,44]. Moreover, metallic electrodes show poor adhesion with soft dielectrics sandwiched between them resulting in low output current [45]. Carbon based electrodes avails themselves an excellent alternative against metals due to increased flexibility, adhesion, and porosity [46,47]. Several carbon-based materials like graphene, few 2D materials and carbon nanotubes etc. have been implicated as back electrodes in TENGs [48]. Graphene amidst all 2D materials shows excellent properties of flexibility, transparency and thermal stability (fig 1b and 1c) makes itself as an ideal option as electrode material for smart TENGs [49]. However pristine graphene films results in low output power density and pursues surface alterations to enhance overall efficiency[50]. In this regard we summarize various methods to improve the quality of graphene films and their use as electrodes in triboelectric nanogenerators. It is confirmed that replacing the conventional metal electrodes with graphene films, graphene-based polymer composite electrodes, and laser induced graphene electrodes improves the output power density. Various methods of functionalizing graphene

films with conducting polymers, designing, and transplanting films for flexible devices, and their uses as electrodes are discussed.

Recent reports and results which emphasize more on the electrode selection for better performance of the triboelectric nanogenerator device are also discussed.

2. Surface modelling of graphene electrodes

Graphene can be produced by a variety of techniques like scotch tape, Liquid phase exfoliation, CVD, Hummer's method, Laser induced etc [51,52]. Exfoliated graphene and functionalized graphene films show potential applications in energy storage, and smart electronics especially in energy harvesting devices like PENGs and TENGs [53]. In this section, various methods of surface engineering of graphene films and their role as electrodes for enhanced performance of TENGs are demonstrated. A qualitative comparison of pristine graphene electrode, graphene–polymer composite and laser-induced graphene electrode is discussed.

2.1 Exfoliated Graphene films for TENG

2.1.1 Water exfoliated graphene film for single electrode TENG

Among all existing operating modes of TENGs, single electrode mode is widely used because of its wide range of applications and accessible design [54]. Furthermore, to fulfil the requirement of flexible devices, various methods of depositing graphene films on substrates like paper, polymer and fibers have been discussed. These methods require additional incorporation of polymers with graphene and their high temperature demand largely limits the compatibility of flexible devices. Dong-Wook Shin et al. [55] demonstrated a cost-effective process of transferring graphene films on flexible substrate and their use as a single electrode triboelectric nanogenerator. Their process consisted of synthesis of pristine

graphene by shear exfoliation of graphite flakes with water and sodium cholate as surface active agent. Shear exfoliated pristine graphene films composed of IPA (isopropyl alcohol assisted) assisted direct transfer (IDT) process. Exfoliated graphene flakes can easily be transferred to substrates by IDT Schematic diagram of the complete process of exfoliation and deposition is depicted in figure 4. Further exfoliated pristine graphene film is transferred to PET substrate by IDT method. Polydimethylsiloxane (PDMS) is deposited on graphene film by drop casting method.

Finally, a flexible and semi-transparent device for a single-electrode triboelectric nanogenerator is fabricated which is shown in figure 5(a). When human fingers or skin are brought in full contact of PDMS then they get positively and negatively charged respectively due to their difference in electronegativity. Electric potential difference is generated as the contact status between the two tribo materials is repeatedly changing. This in turn causes a short, circuited current to flow across the circuit as a consequence of exchange of electrons between ground and shear exfoliated graphene film electrode. As the cycle of approaching and releasing continuously changing, an open circuited voltage of 1.08V and short-circuited current of 0.25μA recorded as shown in figure 5(b). Further to increase the performance of TENG device characteristics can further be improved by bending the device (figure 5b). Excellent flexibility of as prepared film (fig 5c) and promising response under mechanical movement (5d and5e) can be observed.

2.1.2 Shear Exfoliated Graphene electrodes

To implement solution-based methods in fabrication of TENGs, Domingos et al. [56] introduced shear-exfoliated graphene electrodes to enhance the flexibility of the device. SEG flakes were obtained from graphite by solution-processed method using sodium cholate as

surfactant. Two TENG devices were fabricated using graphene and aluminium as back electrodes in order to compare the performance of metal and carbon electrodes [56]. Figure 6 a show the fabrication of two TENG devices with SEG and Al as back electrodes with PDMS and Polyimide as tribonegative and tribopositive materials respectively. The triboelectric response of SEG electrode-based device showed open circuited potential of V_{oc} value of 233V and I_{sc} of 731nA (fig 6b). A maximum power density of 13.14 $\mu W/cm^2$ is achieved which is 40 times higher than that from aluminium electrodes based TENG.

These methods pertain a variety of scopes of using graphene sheets or films as electrodes for future realization of flexible and high performance TENGs as exfoliated sheets tend to increase surface to volume ratio exposing more contact area than pristine graphene. Moreover, graphene-based electrodes insinuate use of other carbon materials over metal electrodes to aid the textile and wearable applications of TENG. However less conductivity, high quality of exfoliated sheets, transplantation of graphene films and low yield of product are still a major challenge to get the higher output in case of graphene films [57]. Creating active sites through tribo surface to expose more area by suitable doping can be a superior choice.

2.2 Nitrogen doped graphene electrodes

Chemical and electronic properties of tribomaterials and respective electrodes are equally important in improving the TENG performance. In this regard Pace et al. [58] highlighted the fundamental role played by electrode capacitance in boosting the overall performance of TENG. Electrode capacitance can be improved by suitable doping of materials which can create active sites within tribo surface and ease the charge transfer. In this regard, few layers graphene (FLG) electrodes based flexible TENG device is fabricated along with nylon and PVDF as tribomaterials. An interlayer of N doped graphene samples dispersed into

Polyurethane glue for better adhesion is inserted in-between to increase the electrode capacitance which is shown in figure 7a. Three different samples of N doped graphene namely N1, N2 and r-N were synthesized through various methods [58] with different nitrogen concentrations in order to investigate the minimal electronic transport during the charge transfer process in TENG (fig 7). Instant power enhancement is demonstrated when the N doped graphene interlayer is sandwiched between positive triboelectric material and FLG electrode (figure 7b) due to increased electrode capacitance.

This work not only attributes towards focussing on creating electroactive sites within tribomaterials or electrodes to ease the charge flow but also realizes versatile application of exfoliated or few layers graphene films in TENGs. However, electroactive sites do not increase the electrical conductivity and further requires surface monitoring. So, modification of graphene surface to enhance the overall efficiency is still ongoing. Conducting polymer incorporated graphene films can be one such competent tool which not only increases the conductivity but also aids the overall flexibility of devices [59]. Polymer based graphene composite electrodes are an excellent alternative for conventional metal electrodes due to their light weight, high durability, and ease of fabrication [60].

2.3 Graphene – conducting polymer composite based electrodes

Yang *et al.* [61] suggested flexible, transparent and highly efficient TENGs by selecting graphene-based polymer composite as electrodes. Graphene and conductive polymer Poly (3, 4-ethylenedioxythiophene) polystyrene sulfonate (PEDOT: PSS) were mixed and fabricated as electrodes after depositing graphene on PET substrate. Output current density and power of such TENG were increased by a factor of 140% and 118% respectively as compared with pristine graphene electrode due to increased conductivity, decreased charge transfer resistance between electrodes [61]. PEDOT: PSS (Clevious PH1000, Heraeus) was deposited

on graphene film by spin coating method at different rpm. All mixtures of graphene with PH100 were entitled as PET Gr/P -1k, Gr/P-3k, Gr/P-5k according to deposition rate 1000rpm, 3000rpm and 5000 rpm respectively. Fabrication, transparency, and output characteristics of the device is shown in figure 8. Current density and voltage of pristine graphene and graphene-based polymer composite electrodes are compared (figure 9) and it is verified that current density of pristine graphene increases from 1.0 $\mu A/cm^2$ to 2.4 $\mu A/cm^{2.}$ Similarly, the voltage surges from 26 V to 52 V corresponding to an increase by a factor of 200 %. However the transparency rate of composite electrode is little less than the pristine graphene electrode [61] as shown in figure 8(b). Improved performance of the device can be justified by the fact that the addition of conductive polymer increases the capacity of the device to transport charge within itself [61]. Moreover, such inclusion of polymers makes the surface very rough, which in turn enhances the contact electrification

2.4 Laser Induced Graphene electrodes for TENGs

Laser induced graphene electrodes are another potential candidate in series of carbon-based electrodes which can certainly promotes the flexibility, durability, and portability of TENG devices [62]. Scribing a suitable pulsed laser on carbon sources like paper, cork, polyimide etc. results in photothermal transformation of sp^3 bonded carbon atoms to three-dimensional multi-network which consists of sp^2 bonded carbon atoms which corresponds to LIG films [63]. Laser induced graphene electrodes can be considered as promising agent in optimizing the efficiency of TENGs due to their excellent electrical conductivity, robustness, easy fabrication process, multiple architecture designs, popular tribonegative material and outstanding flexibility [63].

2.4.1 Mxene enabled TENG with LIG electrodes

Mxenes are special class of 2D materials which possess excellent electrical conductivity and high electronegative surface. Moreover, good flexibility of Mxenes meets up the requirement of wearable devices Regarding this Jiang et al. [64] proposed a Mxene enabled TENG device which consists of PDMS/Mxenes as electronegative layer and LIG as electrodes as shown in figure 10. Open circuited voltage and short-circuited current were recorded as 119 V and 11 μA respectively for the proposed TENG configuration (figure 10). Also output power density surged to 601.9 mW/cm^2. LIG electrodes plays a vital role not only in improving the flexibility but also in enhancing the overall electrical conductivity. Flexibility of as prepared TENG has been verified after successful trial to harvest leaf swing energy [64]. Also, such configuration is useful in harvesting mechanical energy from human motion which fulfils the requirement of self-powered sensors. Such inventive design not only facilitates in energy harvesting from ubiquitous mechanical movement but can be applicable in real time trajectory and self-sensing applications.

2.4.2 LIG based metal TENG

Michael G. Stanford et al [65] fabricated laser induced graphene electrodes on various substrates and compared the output performance of TENGs. A vertical contact design of one such device using LIG is shown in figure 11. Polyamide and aluminium having large difference in their electronegativity were chosen as two active triboelectric materials, which in turn triggered the output power density. Open circuited voltage and short-circuited current of such device was recorded in the range from -600 V to 3500 V and ~60 μA respectively. Metal electrodes-based devices certainly enhances the output power due to increased conductivity and higher ion mobility but have disadvantages in implantation of flexible TENGs.

2.4.3 LIG based metal free TENGs

A flexible, metal free and single electrode mode TENG device is shown in figure 12. Human skin and LIG coated PDMS were chosen as active tribo materials to configure in a single electrode mode. Laser induced graphene layer is connected to ground [65]. Open circuited voltage ~ 300 V and ~ 1.2 mW output power were recorded. Strength of different materials is compared against PDMS (figure 12c) and their response for open circuit voltage was recorded. Skin and nitrile-based device showed better efficiency than aluminium and borosilicate. Another subsequent report on metal free electrodes [44] in TENG device using paper-LIG and PI-LIG shows V_{pp}~ 625 V and instantaneous power density of 2.25 W m^{-2} which is significantly higher than the value reported for LIG electrode by Stanford et al. [65]. With careful observation and literature survey it can be concluded that though exfoliated graphene, doped graphene, graphene composites electrodes relatively increase the output efficiency of TENGs upto certain extent, but LIG electrodes owes maximum efficiency among them.

Table 1 shows a qualitative comparison of output performance of various graphene electrode based TENGs

Type of electrode	Configuration mode	Substrate	Open circuited voltage (V)	Short-circuited current	Current Density (μA /cm^2)	Output power or power density	Reference
Water exfoliated graphene electrode	Single electrode mode	PET	1.08	0.25 μA		-	**51**
Plasma treated water exfoliated graphene electrode	Single electrode mode	PET	4.98	0.52 μA		-	**51**
Pristine Graphene	Vertical contact mode	PET	26	-	1.0		**51**
Shear Exfoliated Graphene electrodes	Vertical contact mode		233V	731 nA		13.14 μW/cm^2	**52**
Graphene-PEDOT: PSS composite electrode (Gr/P-1k)	Vertical contact mode	PET	52		2.4		**57**
Nitrogen doped graphene electrodes	Vertical contact mode	-	-	-	-	122 μW	**54**
Mxene based LIG modified electrode	Single electrode mode	Polyimide	119	11 μA		601.9 mW/cm^2	**60**
Metal free LIG electrodes	Single electrode mode	PDMS	~ 300	10 μA		0.33W/cm^2	**61**
Metal free LIG electrodes	Vertical contact mode	Polyimide	~ 625V	-		2.25 W/m^2	**40**
Metal based LIG electrodes	Vertical contact mode	Aluminium	~3500	60 μA		2.4 W/m^2	**61**

2.4.4 Why LIG electrodes increases performance of TENG?

Laser induced graphene is usually preferred over conventional pristine graphene due to its tuneable designing techniques [66] which in turn opens a scope for fabricating interdigital electrode pattering for TENG. Moreover, porosity of electrode is a crucial factor in

improving the performance of TENG devices [67]. Laser induced graphene designed by irradiation of CO_2

laser on Polyimide sheet holds such porous character [66]. So, an enhanced performance of device is expected by fabrication of such micro-porous LIG electrodes over few layer graphene or pristine graphene. To explain the improved performance of TENG fabricated with LIG electrodes, we need to reflect upon the basic mechanism of contact electrification in terms of energy levels. When two tribo materials with different electron affinity come in contact with each other, they exchange charges which is determined by their fermi levels (E_F) and different work function [68–70]. A material with higher work function has high electron affinity whereas material with lower work function has lower electron affinity [70]. It is believed that for vertical contact mode TENG device, difference in work function of two tribo materials is crucial in improving the output power [70]. A large difference in working functions of two materials drives significant amount of charge density which in turn enhances the electrical output of TENG [70]. Moreover, a difference in work function establishes a built-in potential (V_{bi}) inside a TENG device which aids the output characteristics [71]. Further to understand the movement of charge at the interface of two materials we need to consider the surface state model suggested by Cheng Xu et.al [26]. For charge transfer between two contacting materials, barrier height of material's surface plays a vital role[26]. The process of altering the barrier height by changing the contact materials is termed as regulation which can further be attributed to work function [26]. A schematic diagram explaining the basic mechanism of surface state model during the contact of two materials is shown in figure 13a-f. Regulation of potential barrier height during the contact of metal and dielectric is displayed in figure 13a-c while for dielectric–dielectric contact is shown from 13d-f. Initially when there is no contact between metal and dielectric, neutral energy states E_n in the dielectric is at same level as the fermi level E_f in metal. During the contact of two

materials, some electrons will jump from dielectric by overcoming the barrier height W into the metal surface. As shown in figure 13b, if metal has higher work function, then there will be difference ΔE between neutral states E_n and fermi level $E_{f.}$ with E_n being lower than E_f. During such contact electron encounters a small barrier of height W-ΔE. Similarly, if the metal has the lower work function, then its fermi level $E_{f.}$ will be ΔE lower than the neutral states E_n figure 13c. For electron to transfer from dielectric to metal, it must cross a greater barrier of W+ΔE. Similarly, regulation of potential barrier for dielectric- dielectric interface is displayed in figure 13d-f. High electrical output of metal LIG based TENG [65] can be explained with the help of surface state model and difference of work function of two contacting materials. In case of LIG/PI/Al based TENG device [65], on the PI/Al side, large difference in work function between the metal and dielectric interface will drive significant amount of initial charge .While LIG/PI side lacks any initial charge due to near matching of work functions [44]. So, PI/Al side can be assumed as tribo positive material due to its charge providing nature whereas LIG/PI acts as tribo negative materials due to its charge accepting nature[71]. Thus PI/Al side with some initial charge and LIG/PI with no significant charge lowers the barrier height W by ΔE and which further enhance the electrical output of TENG.

2.4.5 Potential applications based on graphene electrodes

Graphene based TENGs holds flexible and transparent character which supports the progress of real time implantable devices. Yang et al. [61]. used graphene-based polymer composite electrodes to monitor the motion signal from human finger joints at different bending angles. This approach opens a broad range of ideas to fabricate devices which can monitor the motion signals from other parts of human body.

Jiang et al. [64]. utilized daily routine process to harvest mechanical energy using laser induced graphene electrodes-based device. As designed single electrode mode device used as

a writing board to harvest writing energy. Charge flow continue between LIG electrode and ground depending on the writing state. Such type of design can effectively use the wasted writing energy in daily life. In another report, harvesting mechanical energy from human movement based on single electrode mode [65] is shown in figure 14. LIG coated PDMS and human skin were chosen as active tribo material and connected through a circuit into heels (figure 8c). Open circuited voltage of 760 V recorded when LIG/PDMS brought into contact with skin (figure8g).

Conclusions and Future scopes:

This review summarizes and broadly highlights the recent advances in graphene electrodes enabled TENG devices and the corresponding mechanism for enhanced output characteristics. Graphene based TENGs are not only capable to increase the device flexibility and conductivity but also accountable for remarkable mechanical properties, large specific area and robustness. Although a substantial amount of research progress has been achieved on graphene based TENGs, but it still seeks several challenges for overall development. Poor quality of produced graphene films and long, tedious, and costly synthesis process of obtaining these films makes the implantation process really sophisticated in real time TENG devices. Thus, production of easy and delectable method to obtain graphene is still a key challenge. Surface modifications to make graphene as charge enrich material and rational design techniques of graphene electrodes can drastically change the output power of TENGs. Designing the device consisting of crumpled graphene electrode [72] which makes the surface rough and wrinkled, indicates new steps of evolution of such electrodes. Also, permittivity of a substrate plays vital role in aiding the output power of the device. Incorporation of charge enrich tribo material on low permittivity substrate increases the efficiency of device [73]. Thus, new generations flexible TENGs can be accessed by encompassing of graphene on low permittivity substrate. An inventive and more enhanced

design of interdigital electrode [74] inspires same investigation in graphene surface for future TENGs. Laser induced graphene-based devices apart from accessible design and tremendous output performances [65] also realizes a wide range of applications including portability and durability. Moreover, lack of theoretical insight in charge transfer between graphene electrodes and tribomaterials is a major constraint in designing high efficiency TENG devices. So, a detailed investigations on the fundamental charge storage and transfer by graphene electrodes in triboelectrification can guide towards fabricating of high energy conversion TENG devices. Also, stability, durability and robustness of as prepared electrodes is a major concern due to harsh environmental conditions like lack of suitable temperature and high humidity. A better control system over these physical parameters can not only lead to sustainable, compact, and superior TENGs but also enhances the probability of implementing them in human health and safety purposes through textile and wearable systems. Overall, development of energy harvesting devices and nanotechnology has bright future with laydown of materials like graphene.

Conflict of Interests:

The authors declare that they have no conflict of interests.

Acknowledgments:

Deepak Deepak acknowledges the financial support from Shiv Nadar Institution of Eminence, India for the financial support through the scholarship.

References

[1] Q. Zhang, Z. Zhang, Q. Liang, F. Gao, F. Yi, M. Ma, Q. Liao, Z. Kang, Y. Zhang, Green hybrid power system based on triboelectric nanogenerator for wearable/portable electronics, Nano Energy. 55 (2019) 151–163.

https://doi.org/10.1016/j.nanoen.2018.10.078.

[2] H.K. Hong, C.H. Kwon, S.R. Kim, D.H. Yun, K. Lee, Y.K. Sung, Portable electronic nose system with gas sensor array and artificial neural network, Sensors Actuators, B Chem. 66 (2000) 49–52. https://doi.org/10.1016/S0925-4005(99)00460-8.

[3] Y.C. Lai, B.W. Ye, C.F. Lu, C.T. Chen, M.H. Jao, W.F. Su, W.Y. Hung, T.Y. Lin, Y.F. Chen, Extraordinarily Sensitive and Low-Voltage Operational Cloth-Based Electronic Skin for Wearable Sensing and Multifunctional Integration Uses: A Tactile-Induced Insulating-to-Conducting Transition, Adv. Funct. Mater. 26 (2016) 1286–1295. https://doi.org/10.1002/adfm.201503606.

[4] Q. Shi, Z. Sun, Z. Zhang, C. Lee, Triboelectric Nanogenerators and Hybridized Systems for Enabling Next-Generation IoT Applications, Research. 2021 (2021) 1–30. https://doi.org/10.34133/2021/6849171.

[5] Y. Zou, V. Raveendran, J. Chen, Wearable triboelectric nanogenerators for biomechanical energy harvesting, Nano Energy. 77 (2020) 105303. https://doi.org/10.1016/j.nanoen.2020.105303.

[6] X. Ren, H. Fan, C. Wang, J. Ma, S. Lei, Y. Zhao, H. Li, N. Zhao, Magnetic force driven noncontact electromagnetic-triboelectric hybrid nanogenerator for scavenging biomechanical energy, Nano Energy. 35 (2017) 233–241. https://doi.org/10.1016/j.nanoen.2017.03.047.

[7] A.R. Dehghani-Sanij, E. Tharumalingam, M.B. Dusseault, R. Fraser, Study of energy storage systems and environmental challenges of batteries, Renew. Sustain. Energy Rev. 104 (2019) 192–208. https://doi.org/10.1016/j.rser.2019.01.023.

[8] S. Schismenos, M. Chalaris, G. Stevens, Battery hazards and safety: A scoping review

for lead acid and silver-zinc batteries, Saf. Sci. 140 (2021) 105290. https://doi.org/10.1016/j.ssci.2021.105290.

[9] Z. Zhu, H. Xiang, Y. Zeng, J. Zhu, X. Cao, N. Wang, Z.L. Wang, Continuously harvesting energy from water and wind by pulsed triboelectric nanogenerator for self-powered seawater electrolysis, Nano Energy. 93 (2022) 106776. https://doi.org/10.1016/j.nanoen.2021.106776.

[10] J. Luo, S. Zhang, M. Sun, L. Yang, S. Luo, J.C. Crittenden, A Critical Review on Energy Conversion and Environmental Remediation of Photocatalysts with Remodeling Crystal Lattice, Surface, and Interface, ACS Nano. 13 (2019) 9811–9840. https://doi.org/10.1021/acsnano.9b03649.

[11] R. Morais, S.G. Matos, M.A. Fernandes, A.L.G. Valente, S.F.S.P. Soares, P.J.S.G. Ferreira, M.J.C.S. Reis, Sun, wind and water flow as energy supply for small stationary data acquisition platforms, Comput. Electron. Agric. 64 (2008) 120–132. https://doi.org/10.1016/j.compag.2008.04.005.

[12] M. Mariello, F. Guido, V.M. Mastronardi, M.T. Todaro, D. Desmaële, M. De Vittorio, Nanogenerators for harvesting mechanical energy conveyed by liquids, Nano Energy. 57 (2019) 141–156. https://doi.org/10.1016/j.nanoen.2018.12.027.

[13] S.T. Yusuf, Y.M.A. Halim, A.S. Samosir, M. Abdulkadir, Mechanical energy harvesting devices for low frequency applications: Revisited, ARPN J. Eng. Appl. Sci. 8 (2013) 504–512.

[14] L. Liu, X. Guo, C. Lee, Promoting smart cities into the 5G era with multi-field Internet of Things (IoT) applications powered with advanced mechanical energy harvesters, Nano Energy. 88 (2021) 106304. https://doi.org/10.1016/j.nanoen.2021.106304.

[15] X. Ren, H. Fan, C. Wang, J. Ma, N. Zhao, Coaxial rotatory-freestanding triboelectric nanogenerator for effective energy scavenging from wind, Smart Mater. Struct. 27 (2018) 65016. https://doi.org/10.1088/1361-665X/aabe04.

[16] Y. Zi, Z.L. Wang, Nanogenerators: An emerging technology towards nanoenergy, APL Mater. 5 (2017). https://doi.org/10.1063/1.4977208.

[17] T. Cheng, Q. Gao, Z.L. Wang, The Current Development and Future Outlook of Triboelectric Nanogenerators: A Survey of Literature, Adv. Mater. Technol. 4 (2019) 1–7. https://doi.org/10.1002/admt.201800588.

[18] A. Ahmed, I. Hassan, A.S. Helal, V. Sencadas, A. Radhi, C.K. Jeong, M.F. El-Kady, Triboelectric Nanogenerator versus Piezoelectric Generator at Low Frequency (<4 Hz): A Quantitative Comparison, IScience. 23 (2020) 101286. https://doi.org/10.1016/j.isci.2020.101286.

[19] X. Xie, Y. Zhang, C. Chen, X. Chen, T. Yao, M. Peng, X. Chen, B. Nie, Z. Wen, X. Sun, Frequency-independent self-powered sensing based on capacitive impedance matching effect of triboelectric nanogenerator, Nano Energy. 65 (2019) 103984. https://doi.org/10.1016/j.nanoen.2019.103984.

[20] Z.L. Wang, J. Chen, L. Lin, Progress in triboelectric nanogenerators as a new energy technology and self-powered sensors, Energy Environ. Sci. 8 (2015) 2250–2282. https://doi.org/10.1039/c5ee01532d.

[21] G. Zhu, B. Peng, J. Chen, Q. Jing, Z. Lin Wang, Triboelectric nanogenerators as a new energy technology: From fundamentals, devices, to applications, Nano Energy. 14 (2014) 126–138. https://doi.org/10.1016/j.nanoen.2014.11.050.

[22] X. Ren, H. Fan, C. Wang, J. Ma, H. Li, M. Zhang, S. Lei, W. Wang, Wind energy

harvester based on coaxial rotatory freestanding triboelectric nanogenerators for self-powered water splitting, Nano Energy. 50 (2018) 562–570. https://doi.org/10.1016/j.nanoen.2018.06.002.

[23] H.J. Yoon, H. Ryu, S.W. Kim, Sustainable powering triboelectric nanogenerators: Approaches and the path towards efficient use, Nano Energy. 51 (2018) 270–285. https://doi.org/10.1016/j.nanoen.2018.06.075.

[24] R. Hinchet, A. Ghaffarinejad, Y. Lu, J.Y. Hasani, S.W. Kim, P. Basset, Understanding and modeling of triboelectric-electret nanogenerator, Nano Energy. 47 (2018) 401–409. https://doi.org/10.1016/j.nanoen.2018.02.030.

[25] S. Niu, Z.L. Wang, Theoretical systems of triboelectric nanogenerators, Nano Energy. 14 (2014) 161–192. https://doi.org/10.1016/j.nanoen.2014.11.034.

[26] C. Xu, Y. Zi, A.C. Wang, H. Zou, Y. Dai, X. He, P. Wang, Y.C. Wang, P. Feng, D. Li, Z.L. Wang, On the Electron-Transfer Mechanism in the Contact-Electrification Effect, Adv. Mater. 30 (2018) 1–9. https://doi.org/10.1002/adma.201706790.

[27] Z.L. Wang, Triboelectric nanogenerators as new energy technology and self-powered sensors - Principles, problems and perspectives, Faraday Discuss. 176 (2014) 447–458. https://doi.org/10.1039/c4fd00159a.

[28] Khushboo, P. Azad, Triboelectric nanogenerator based on vertical contact separation mode for energy harvesting, Proceeding - IEEE Int. Conf. Comput. Commun. Autom. ICCCA 2017. 2017-Janua (2017) 1499–1502. https://doi.org/10.1109/CCAA.2017.8230037.

[29] Z.L. Wang, L. Lin, J. Chen, S. Niu, Y. Zi, Triboelectric Nanogenerator: Lateral Sliding Mode, 2016. https://doi.org/10.1007/978-3-319-40039-6_3.

[30] W. Shang, G.Q. Gu, F. Yang, L. Zhao, G. Cheng, Z.L. Du, Z.L. Wang, A Sliding-Mode Triboelectric Nanogenerator with Chemical Group Grated Structure by Shadow Mask Reactive Ion Etching, ACS Nano. 11 (2017) 8796–8803. https://doi.org/10.1021/acsnano.7b02866.

[31] G. Zhu, B. Peng, J. Chen, Q. Jing, Z. Lin Wang, Triboelectric nanogenerators as a new energy technology: From fundamentals, devices, to applications, Nano Energy. 14 (2014) 126–138. https://doi.org/10.1016/j.nanoen.2014.11.050.

[32] Y. Wang, Y. Yang, Z.L. Wang, Triboelectric nanogenerators as flexible power sources, Npj Flex. Electron. 1 (2017) 1–9. https://doi.org/10.1038/s41528-017-0007-8.

[33] S. Wang, Y. Xie, S. Niu, L. Lin, Z.L. Wang, Freestanding triboelectric-layer-based nanogenerators for harvesting energy from a moving object or human motion in contact and non-contact modes, Adv. Mater. 26 (2014) 2818–2824. https://doi.org/10.1002/adma.201305303.

[34] D. Godwinraj, S.C. George, Recent advancement in TENG polymer structures and energy efficient charge control circuits, Adv. Ind. Eng. Polym. Res. 4 (2021) 1–8. https://doi.org/10.1016/j.aiepr.2020.12.003.

[35] D.W. Kim, J.H. Lee, J.K. Kim, U. Jeong, Material aspects of triboelectric energy generation and sensors, NPG Asia Mater. 12 (2020). https://doi.org/10.1038/s41427-019-0176-0.

[36] X. Ren, H. Fan, J. Ma, C. Wang, Y. Zhao, S. Lei, Triboelectric nanogenerators based on fluorinated wasted rubber powder for self-powering application, ACS Sustain. Chem. Eng. 5 (2017) 1957–1964. https://doi.org/10.1021/acssuschemeng.6b02756.

[37] Y. Liu, J. Mo, Q. Fu, Y. Lu, N. Zhang, S. Wang, S. Nie, Enhancement of Triboelectric

Charge Density by Chemical Functionalization, Adv. Funct. Mater. 30 (2020) 1–33. https://doi.org/10.1002/adfm.202004714.

[38] M. Lai, B. Du, H. Guo, Y. Xi, H. Yang, C. Hu, J. Wang, Z.L. Wang, Enhancing the Output Charge Density of TENG via Building Longitudinal Paths of Electrostatic Charges in the Contacting Layers, ACS Appl. Mater. Interfaces. 10 (2018) 2158–2165. https://doi.org/10.1021/acsami.7b15238.

[39] R. Hinchet, W. Seung, S.W. Kim, Recent Progress on Flexible Triboelectric Nanogenerators for SelfPowered Electronics, ChemSusChem. 8 (2015) 2327–2344. https://doi.org/10.1002/cssc.201403481.

[40] Y. Zou, L. Bo, Z. Li, Recent progress in human body energy harvesting for smart bioelectronic system, Fundam. Res. 1 (2021) 364–382. https://doi.org/10.1016/j.fmre.2021.05.002.

[41] H. Elahi, K. Munir, M. Eugeni, S. Atek, P. Gaudenzi, Energy harvesting towards self-powered iot devices, Energies. 13 (2020) 1–31. https://doi.org/10.3390/en13215528.

[42] I. Aazem, D.T. Mathew, S. Radhakrishnan, K. V. Vijoy, H. John, D.M. Mulvihill, S.C. Pillai, Electrode materials for stretchable triboelectric nanogenerator in wearable electronics, RSC Adv. 12 (2022) 10545–10572. https://doi.org/10.1039/d2ra01088g.

[43] G. da S. Oliveira, I.C.M. Candido, H.P. de Oliveira, Metal-free triboelectric nanogenerators for application in wearable electronics, Mater. Adv. 3 (2022) 4460–4470. https://doi.org/10.1039/d2ma00195k.

[44] P. Zhao, G. Bhattacharya, S.J. Fishlock, J.G.M. Guy, A. Kumar, C. Tsonos, Z. Yu, S. Raj, J.A. McLaughlin, J. Luo, N. Soin, Replacing the metal electrodes in triboelectric nanogenerators: High-performance laser-induced graphene electrodes, Nano Energy.

75 (2020) 104958. https://doi.org/10.1016/j.nanoen.2020.104958.

[45] N. Inagaki, S. Tasaka, M. Masumoto, Improved adhesion between Kapton film and copper metal by plasma graft polymerization of vinylimidazole, Macromolecules. 29 (1996) 1642–1648. https://doi.org/10.1021/ma9503571.

[46] H. Hwang, K.Y. Lee, D. Shin, J. Shin, S. Kim, W. Choi, Metal-free, flexible triboelectric generator based on MWCNT mesh film and PDMS layers, Appl. Surf. Sci. 442 (2018) 693–699. https://doi.org/10.1016/j.apsusc.2018.02.227.

[47] X. Xia, J. Chen, G. Liu, M.S. Javed, X. Wang, C. Hu, Aligning graphene sheets in PDMS for improving output performance of triboelectric nanogenerator, Carbon N. Y. 111 (2017) 569–576. https://doi.org/10.1016/j.carbon.2016.10.041.

[48] M. Seol, S. Kim, Y. Cho, K.E. Byun, H. Kim, J. Kim, S.K. Kim, S.W. Kim, H.J. Shin, S. Park, Triboelectric Series of 2D Layered Materials, Adv. Mater. 30 (2018) 1–8. https://doi.org/10.1002/adma.201801210.

[49] A.K. Geim, K.S. Novoselov, The rise of graphene, Nanosci. Technol. A Collect. Rev. from Nat. Journals. (2009) 11–19. https://doi.org/10.1142/9789814287005_0002.

[50] F.F. Hatta, M.A.S. Mohammad Haniff, M.A. Mohamed, A review on applications of graphene in triboelectric nanogenerators, Int. J. Energy Res. 46 (2022) 544–576. https://doi.org/10.1002/er.7245.

[51] X.J. Lee, B.Y.Z. Hiew, K.C. Lai, L.Y. Lee, S. Gan, S. Thangalazhy-Gopakumar, S. Rigby, Review on graphene and its derivatives: Synthesis methods and potential industrial implementation, J. Taiwan Inst. Chem. Eng. 98 (2019) 163–180. https://doi.org/10.1016/j.jtice.2018.10.028.

[52] F.M. Vivaldi, A. Dallinger, A. Bonini, N. Poma, L. Sembranti, D. Biagini, P. Salvo, F. Greco, F. Di Francesco, Three-Dimensional (3D) Laser-Induced Graphene: Structure, Properties, and Application to Chemical Sensing, ACS Appl. Mater. Interfaces. 13 (2021) 30245–30260. https://doi.org/10.1021/acsami.1c05614.

[53] P.M. Biranje, A.W. Patwardhan, J.B. Joshi, K. Dasgupta, Exfoliated graphene and its derivatives from liquid phase and their role in performance enhancement of epoxy matrix composite, Compos. Part A Appl. Sci. Manuf. 156 (2022) 106886. https://doi.org/10.1016/j.compositesa.2022.106886.

[54] A.R. Mule, B. Dudem, H. Patnam, S.A. Graham, J.S. Yu, Wearable Single-Electrode-Mode Triboelectric Nanogenerator via Conductive Polymer-Coated Textiles for Self-Power Electronics, ACS Sustain. Chem. Eng. 7 (2019) 16450–16458. https://doi.org/10.1021/acssuschemeng.9b03629.

[55] D.W. Shin, M.D. Barnes, K. Walsh, D. Dimov, P. Tian, A.I.S. Neves, C.D. Wright, S.M. Yu, J.B. Yoo, S. Russo, M.F. Craciun, A New Facile Route to Flexible and Semi-Transparent Electrodes Based on Water Exfoliated Graphene and their Single-Electrode Triboelectric Nanogenerator, Adv. Mater. 30 (2018) 1–7. https://doi.org/10.1002/adma.201802953.

[56] I. Domingos, A.I.S. Neves, M.F. Craciun, H. Alves, Graphene Based Triboelectric Nanogenerators Using Water Based Solution Process, Front. Phys. 9 (2021) 1–8. https://doi.org/10.3389/fphy.2021.742563.

[57] L. Lin, H. Peng, Z. Liu, Synthesis challenges for graphene industry, Nat. Mater. 18 (2019) 520–524. https://doi.org/10.1038/s41563-019-0341-4.

[58] G. Pace, M. Serri, A.E. del R. Castillo, A. Ansaldo, S. Lauciello, M. Prato, L.

Pasquale, J. Luxa, V. Mazánek, Z. Sofer, F. Bonaccorso, Nitrogen-doped graphene based triboelectric nanogenerators, Nano Energy. 87 (2021). https://doi.org/10.1016/j.nanoen.2021.106173.

[59] E.J. Jelmy, D. Jose, K. V. Vijoy, K.J. Saji, H. John, Enhanced triboelectric performance of graphene oxide-conducting polymer hybrid modified polydimethylsiloxane composites, Mater. Adv. 3 (2022) 6897–6907. https://doi.org/10.1039/d2ma00771a.

[60] S. Rana, V. Singh, B. Singh, Recent trends in 2D materials and their polymer composites for effectively harnessing mechanical energy, IScience. 25 (2022) 103748. https://doi.org/10.1016/j.isci.2022.103748.

[61] J. Yang, P. Liu, X. Wei, W. Luo, J. Yang, H. Jiang, D. Wei, R. Shi, H. Shi, Surface Engineering of Graphene Composite Transparent Electrodes for High-Performance Flexible Triboelectric Nanogenerators and Self-Powered Sensors, ACS Appl. Mater. Interfaces. 9 (2017) 36017–36025. https://doi.org/10.1021/acsami.7b10373.

[62] H. Wang, Z. Zhao, P. Liu, X. Guo, Laser-Induced Graphene Based Flexible Electronic Devices, Biosensors. 12 (2022). https://doi.org/10.3390/bios12020055.

[63] H. Chen, W. Yang, P. Huang, C. Li, Y. Yang, B. Zheng, C. Zhang, R. Liu, Y. Li, Y. Xu, J. Wang, Z. Li, A multiple laser-induced hybrid electrode for flexible triboelectric nanogenerators, Sustain. Energy Fuels. 5 (2021) 3737–3743. https://doi.org/10.1039/d1se00819f.

[64] C. Jiang, X. Li, Y. Yao, L. Lan, Y. Shao, F. Zhao, Y. Ying, J. Ping, A multifunctional and highly flexible triboelectric nanogenerator based on MXene-enabled porous film integrated with laser-induced graphene electrode, Nano Energy. 66 (2019) 104121.

https://doi.org/10.1016/j.nanoen.2019.104121.

[65] M.G. Stanford, J.T. Li, Y. Chyan, Z. Wang, W. Wang, J.M. Tour, Laser-Induced Graphene Triboelectric Nanogenerators, ACS Nano. 13 (2019) 7166–7174. https://doi.org/10.1021/acsnano.9b02596.

[66] C.W. Lee, S.Y. Jeong, Y.W. Kwon, J.U. Lee, S.C. Cho, B.S. Shin, Fabrication of laser-induced graphene-based multifunctional sensing platform for sweat ion and human motion monitoring, Sensors Actuators A Phys. 334 (2022) 113320. https://doi.org/10.1016/j.sna.2021.113320.

[67] M. Karimi, S. Seddighi, R. Mohammadpour, Nanostructured versus flat compact electrode for triboelectric nanogenerators at high humidity, Sci. Rep. 11 (2021) 1–15. https://doi.org/10.1038/s41598-021-95621-3.

[68] M. Taghavi, L. Beccai, A contact-key triboelectric nanogenerator: Theoretical and experimental study on motion speed influence, Nano Energy. 18 (2015) 283–292. https://doi.org/10.1016/j.nanoen.2015.10.019.

[69] H. Zou, Y. Zhang, L. Guo, P. Wang, X. He, G. Dai, H. Zheng, C. Chen, A.C. Wang, C. Xu, Z.L. Wang, Quantifying the triboelectric series, Nat. Commun. 10 (2019) 1–9. https://doi.org/10.1038/s41467-019-09461-x.

[70] J. Peng, S.D. Kang, G.J. Snyder, Optimization principles and the figure of merit for triboelectric generators, Sci. Adv. 3 (2017) 1–7. https://doi.org/10.1126/sciadv.aap8576.

[71] C. Xu, B. Zhang, A.C. Wang, W. Cai, Y. Zi, P. Feng, Z.L. Wang, Effects of Metal Work Function and Contact Potential Difference on Electron Thermionic Emission in Contact Electrification, Adv. Funct. Mater. 29 (2019) 1–8.

https://doi.org/10.1002/adfm.201903142.

[72] H. Chen, Y. Xu, L. Bai, Y. Jiang, J. Zhang, C. Zhao, T. Li, H. Yu, G. Song, N. Zhang, Q. Gan, Crumpled Graphene Triboelectric Nanogenerators: Smaller Devices with Higher Output Performance, Adv. Mater. Technol. 2 (2017) 1–7. https://doi.org/10.1002/admt.201700044.

[73] G. Min, L. Manjakkal, D.M. Mulvihill, R.S. Dahiya, Triboelectric Nanogenerator with Enhanced Performance via an Optimized Low Permittivity Substrate, IEEE Sens. J. 20 (2020) 6856–6862. https://doi.org/10.1109/JSEN.2019.2938605.

[74] B. Kil Yun, H. Soo Kim, Y. Joon Ko, G. Murillo, J. Hoon Jung, Interdigital electrode based triboelectric nanogenerator for effective energy harvesting from water, Nano Energy. 36 (2017) 233–240. https://doi.org/10.1016/j.nanoen.2017.04.048.

Figure caption

Figure 1- Schematic diagram of vertical contact mode of TENG

Figure 2. Schematic diagram of electron cloud model explaining the basic mechanism of contact electrification. (a) Electron distribution before contact (b) Transfer of electrons from A to B once they come in contact with each other(c) Trapping of electrons inside B due to potential barrier E_2 after contact status further changed. (d) Charge transfer from B to A as a function of temperature.

Figure 3 shows different working modes of TENG. (a)Vertical contact separation mode, (b) Lateral sliding mode(c) Single electrode mode, (d) Freestanding triboelectric layer mode

Figure4. (a) Shear exfoliation of shear exfoliation of graphite in water and sodium cholate and IDT method. (b) Shear exfoliated samples of graphene with different concentrations (c)

IDT method (d) Exfoliated graphene film in filter membrane is put on an IPA drenched substrate and the detached after heating (e) PET (f) Photograph of glass, (g) paper (h) SiO_2 and (i) Polypropylene fibers

Figure 5. (a) Schematic diagram of working principle of TENG device. (b) V_{OC} and I_{SC} of single electrode mode TENG, pristine graphene exfoliated film, (c) Pictures of flexible device and LED glowing as a result of (d) approaching and (e) releasing.

Figure 6 (a) shows the schematic of SEG/PDMS TENG (bottom left) and Al/PDMS (bottom right) with different components. Figure 6b shows Voltage current behaviour of Al/PDMS and SEG/PDMS. Figure 6c represents qualitative comparison of metal aluminium electrode against flexible graphene electrode.

Figure 7 7a and 7b represents schematic diagram and instant power plot vs resistance of as prepared TENG device from FLG electrodes. 7d and 7e represents Voc as a function of time for different nitrogen doped graphene samples.

Figure 8 (a) Schematic diagram of graphene polymer composite electrode-based device. (b) Transparency rate of device formed (c) Current density comparison of pristine graphene with PH100 mixtures at different rpm (d) Output voltage comparison.

Figure 9. Output plots with load resistors. (a) Variation of voltage with load resistance for pristine graphene(b) Plot of Power with resistance for pristine graphene(c) Variation of voltage with load resistance for modified graphene with PEDOT: POSS(d) Plot of power with resistance for graphene-based polymer composite

Figure 10 Schematic diagram of TENG with PDMS/Mxene composite film with LIG electrodes (a). open circuited voltage and short-circuited current as a function of load

resistance (b) Instantaneous power density as a function of load resistance and turning of 522 LEDS connected in series.

Figure 11. Output performance of metal LIG. (a) Schematic diagram of the device (b) Voc of the device (c) Isc of the device formed (d) Voc and Isc as a function of load (e) Output power as a function of resistance

Figure 12. Performance of LIG metal free TENGs. (a) Schematic of working principle of single electrode TENG (b) Voc of STENG (c) Comparison of Voc of different materials (d) Variation of voltage with load (e) Variation of power with load resistance

Figure13. Schematic diagram showing the basic mechanism of surface state model. (a) Before contact of dielectric and metal, E_n and E_F lies at same level. Charge transfer between metal and dielectric when work function of metal is higher(b) and lower in (c). Before contact of two dielectrics(d) neutral level states lies at same level. Charge transfer mechanism between two dielectrics when work function of one is higher(e) and lower in(f).

Figure 14. Output performance and circuit diagram of LIG based single electrode mode TENG. (a,b) schematic diagram of fabricated device (c) Schematic diagram of circuit of hybrid of single electrode mode TENG flip flop.(d) Separation and contact mode of movement (e) Charging characteristics of different capacitors (f) Walking route showed by map (g) Variation of Voc with time

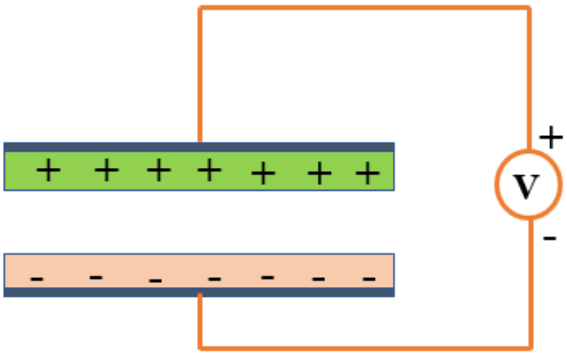

Figure 1 a. Schematic diagram of vertical contact mode of TENG

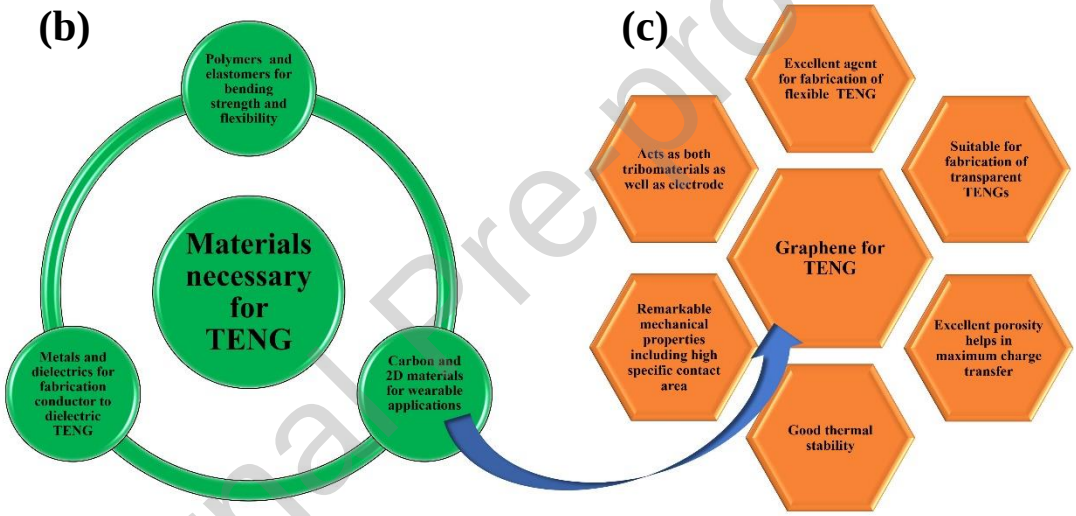

Figure 1 b represents schematic of materials necessary for TENG devices and Fig 1c shows how graphene is suitable for TENGs

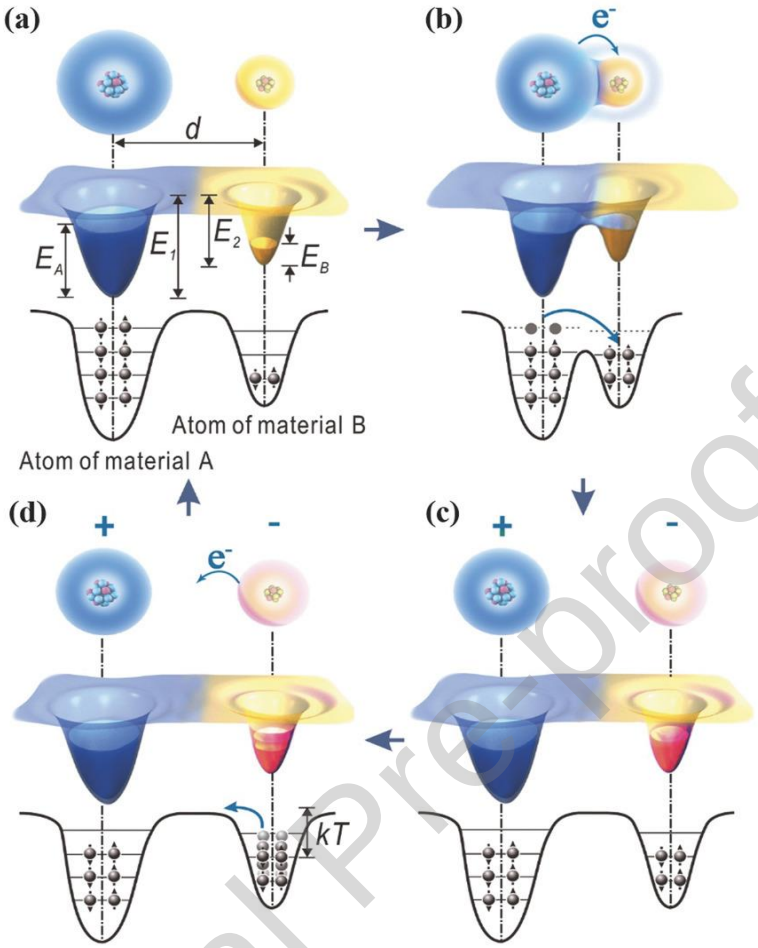

Figure 2. Schematic diagram of electron cloud model explaining the basic mechanism of contact electrification. **Reprinted with permission** [26] (a) Electron distribution before contact (b) Transfer of electrons from A to B once they come in contact with each other(c) Trapping of electrons inside B due to potential barrier E_2 after contact status further changed. (d) Charge transfer from B to A as a function of temperature.

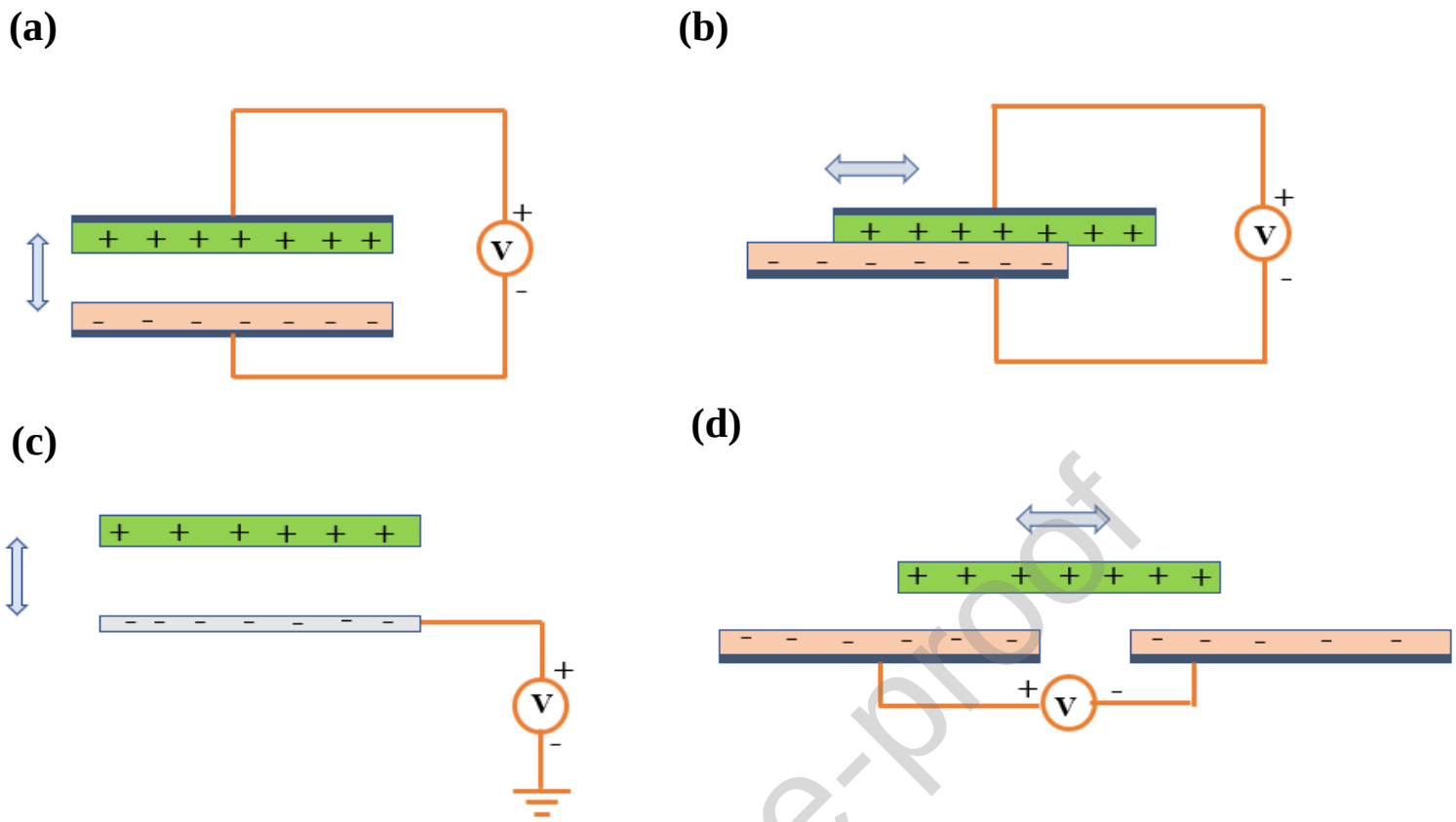

Figure 3 shows different working modes of TENG. (a)Vertical contact separation mode, (b) Lateral sliding mode(c) Single electrode mode, (d) Freestanding triboelectric layer mode

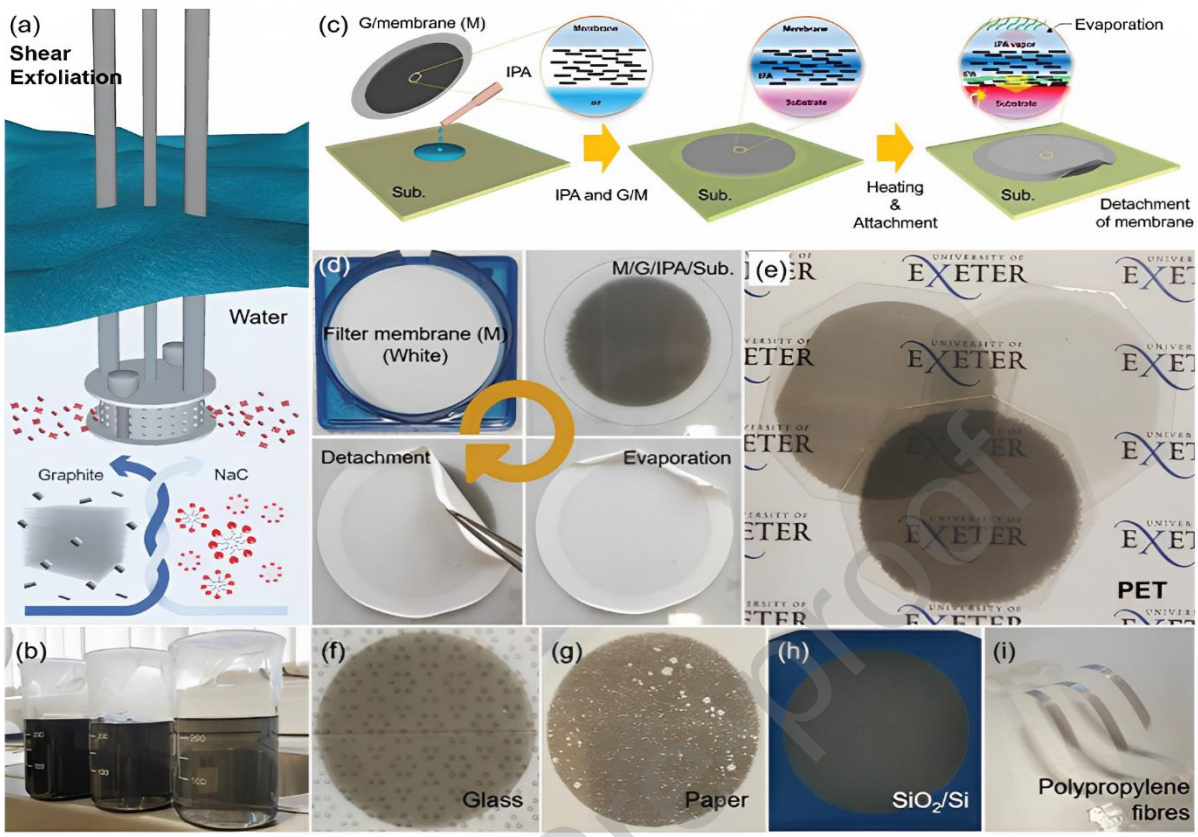

Figure4. (a) Shear exfoliation of shear exfoliation of graphite in water and sodium cholate and IDT method. **Reprinted with permission** [55]. (b) Shear exfoliated samples of graphene with different concentrations (c) IDT method (d) Exfoliated graphene film in filter membrane is put on an IPA drenched substrate and the detached after heating (e) PET (f) Photograph of glass, (g) paper (h) SiO_2 and (i) Polypropylene fibers

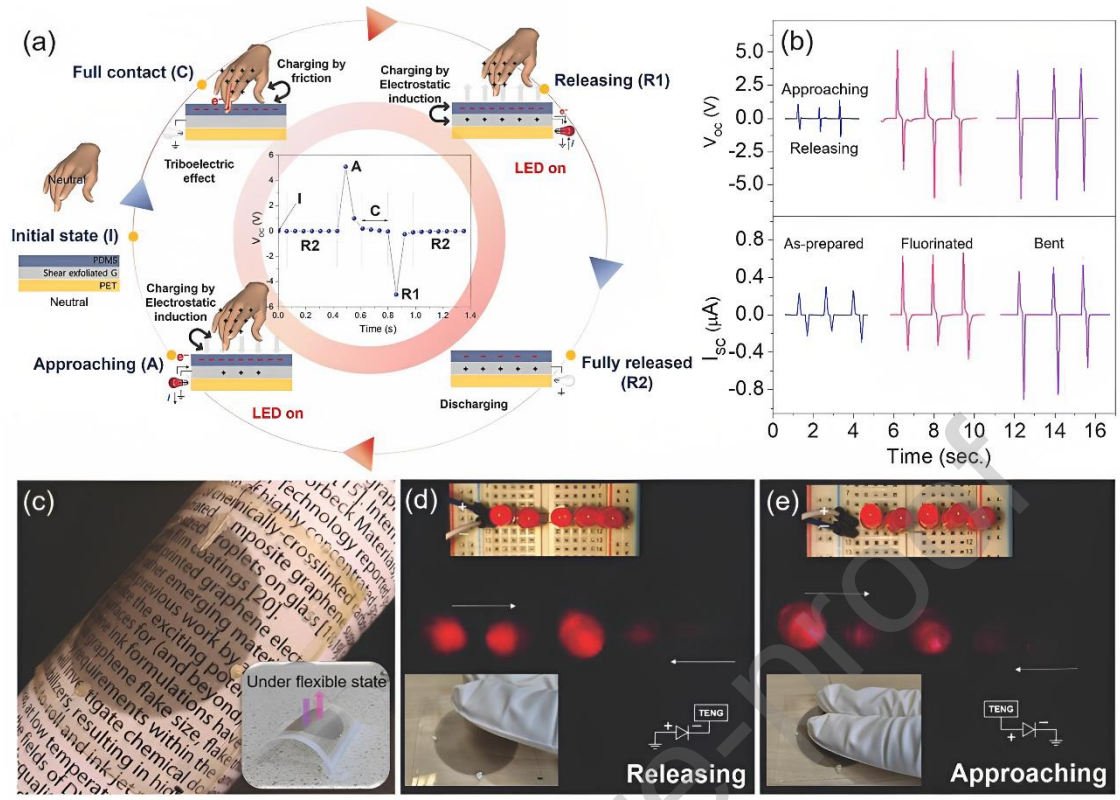

Figure 5. (a) Schematic diagram of working principle of TENG device. **Reprinted with permission** [55]. (b) V_{OC} and I_{SC} of single electrode mode TENG, pristine graphene exfoliated film, (c) Pictures of flexible device and LED glowing as a result of (d) approaching and (e) releasing.

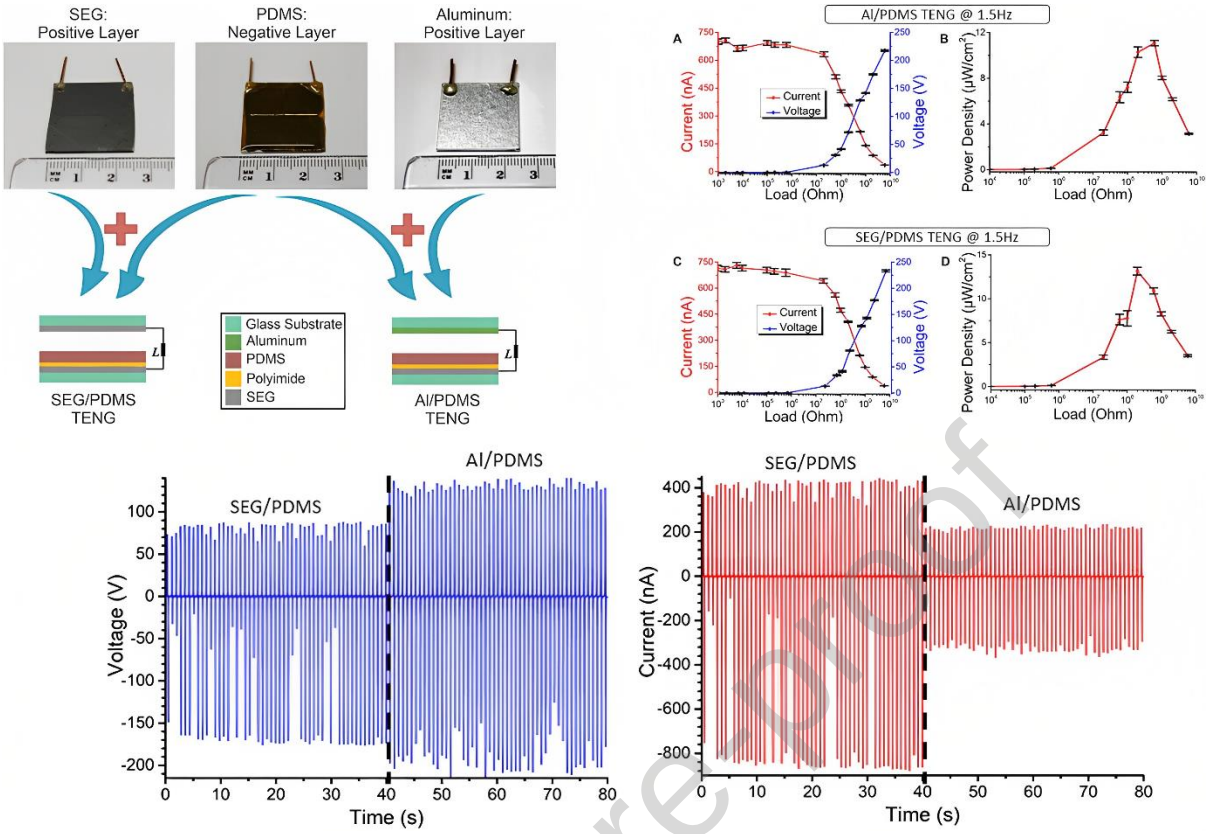

Figure 6. 6a shows the schematic of SEG/PDMS TENG (bottom left) and Al/PDMS (bottom right) with different components. **Reprinted with permission** [56]. Figure 6b shows Voltage current behaviour of Al/PDMS and SEG/PDMS. Figure 6c represents qualitative comparison of metal aluminium electrode against flexible graphene electrode**.**

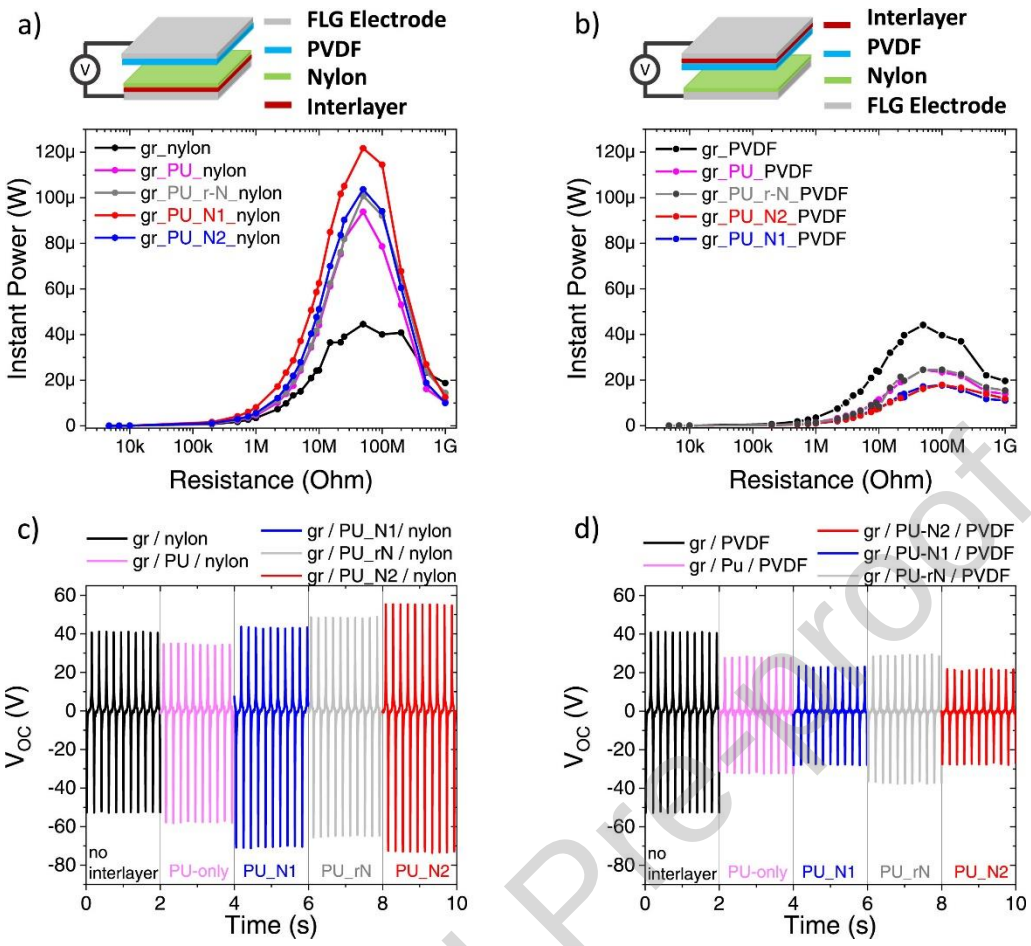

Figure 7. 7a and 7b represents schematic diagram and instant power plot vs resistance of as prepared TENG device from FLG electrodes. 7d and 7e represents Voc as a function of time for different nitrogen doped graphene samples. **Reprinted with permission** [58]

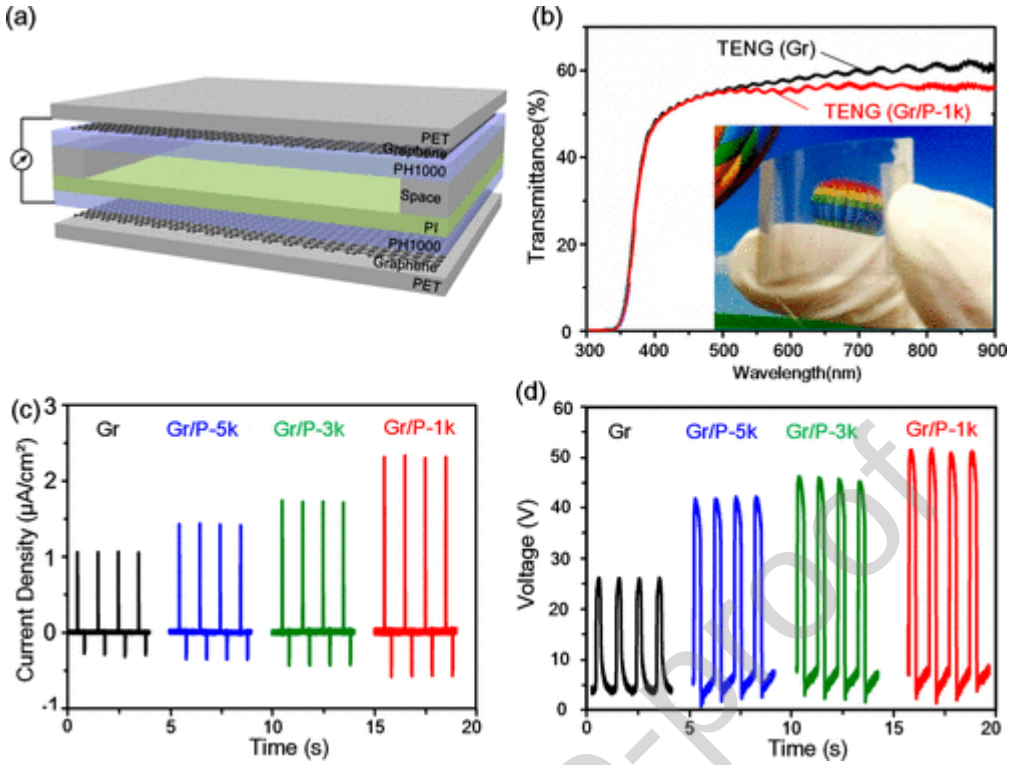

Figure 8. (a) Schematic diagram of graphene polymer composite electrode-based device **Reprinted with permission** [61]. (b) Transparency rate of device formed (c) Current density comparison of pristine graphene with PH100 mixtures at different rpm (d) Output voltage comparison.

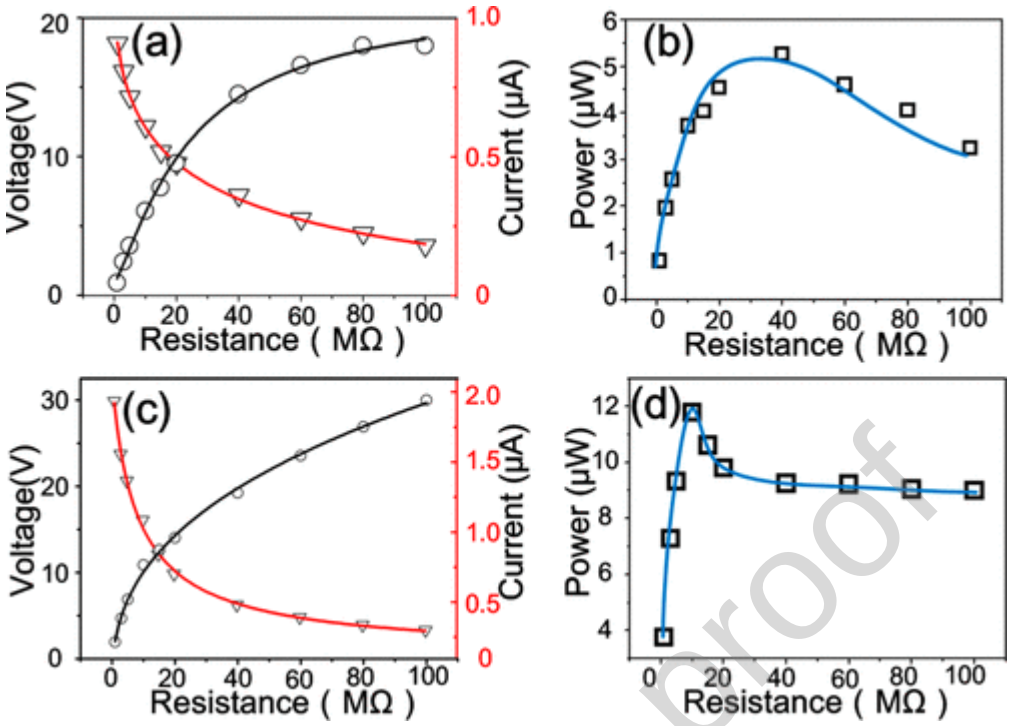

Figure 9. Output plots with load resistors **Reprinted with permission** [61]. (a) Variation of voltage with load resistance for pristine graphene(b) Plot of Power with resistance for pristine graphene(c) Variation of voltage with load resistance for modified graphene with PEDOT: POSS(d) Plot of power with resistance for graphene-based polymer composite

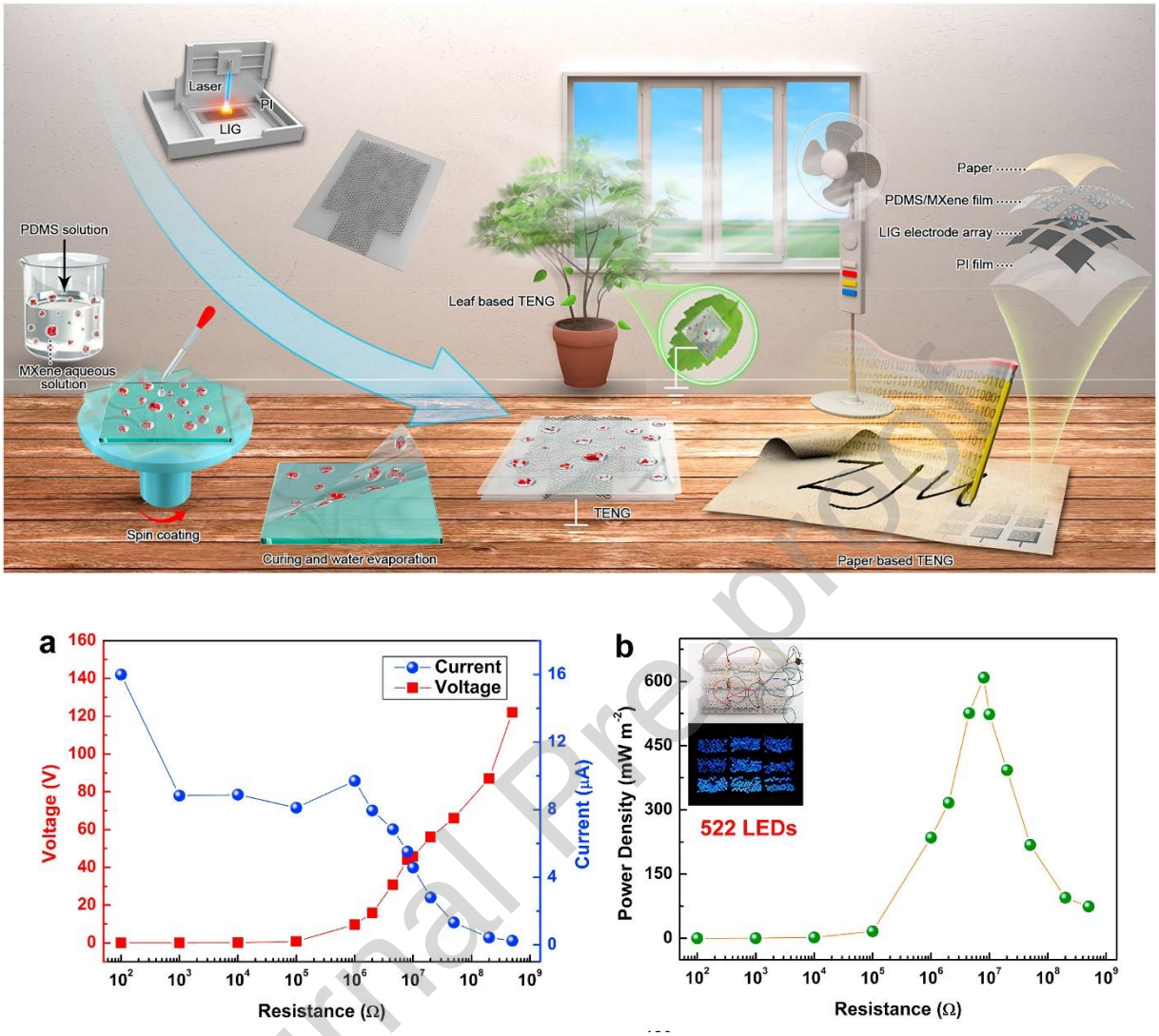

Figure 10 Schematic diagram of TENG with PDMS/Mxene composite film with LIG electrodes **Reprinted with permission** [64] (a). open circuited voltage and short-circuited current as a function of load resistance (b) Instantaneous power density as a function of load resistance and turning of 522 LEDS connected in series.

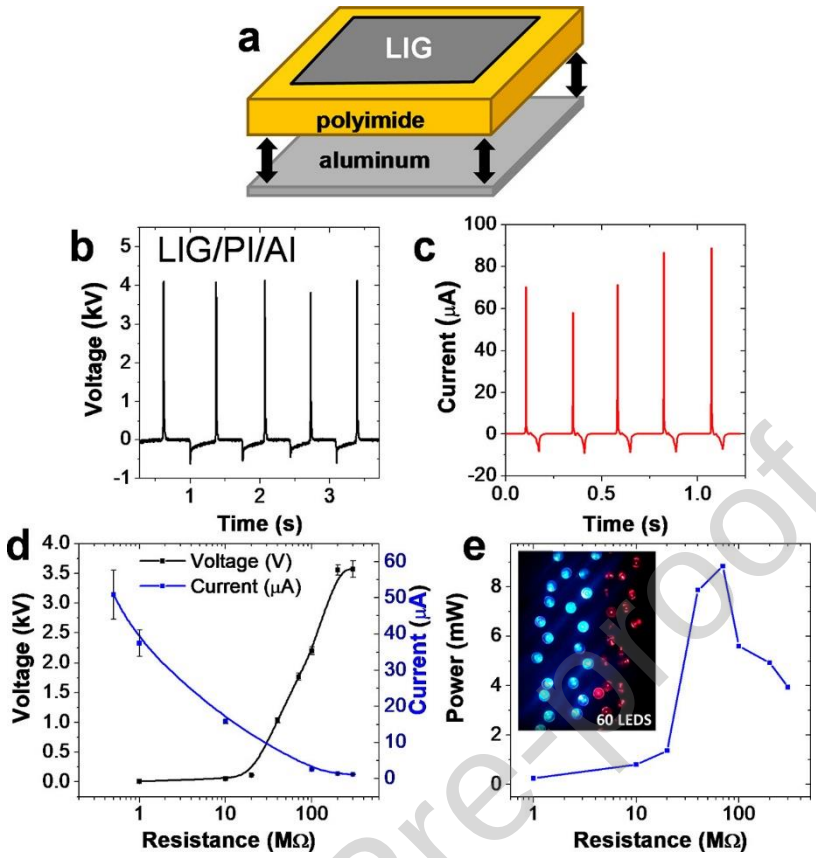

Figure 11. Output performance of metal LIG **Reprinted with permission** [65] (a) Schematic diagram of the device (b) Voc of the device (c) Isc of the device formed (d) Voc and Isc as a function of load (e) Output power as a function of resistance

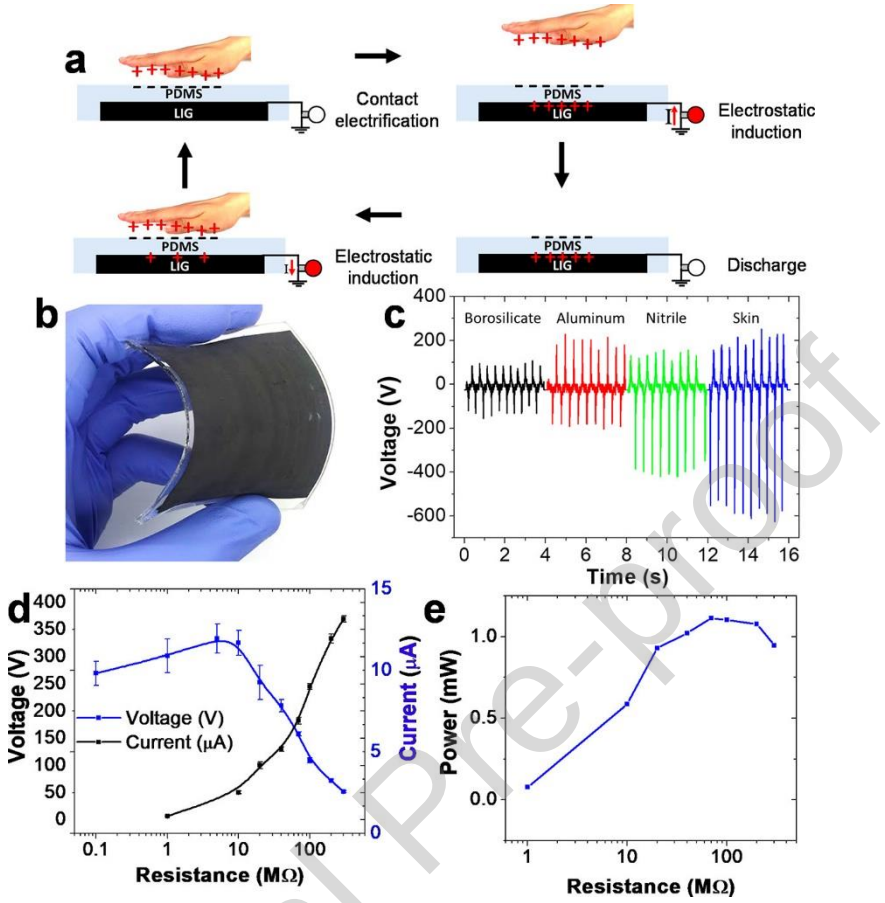

Figure 12. Performance of LIG metal free TENGs **Reprinted with permission** [65]. (a) Schematic of working principle of single electrode TENG (b) Voc of STENG (c) Comparison of Voc of different materials (d) Variation of voltage with load (e) Variation of power with load resistance

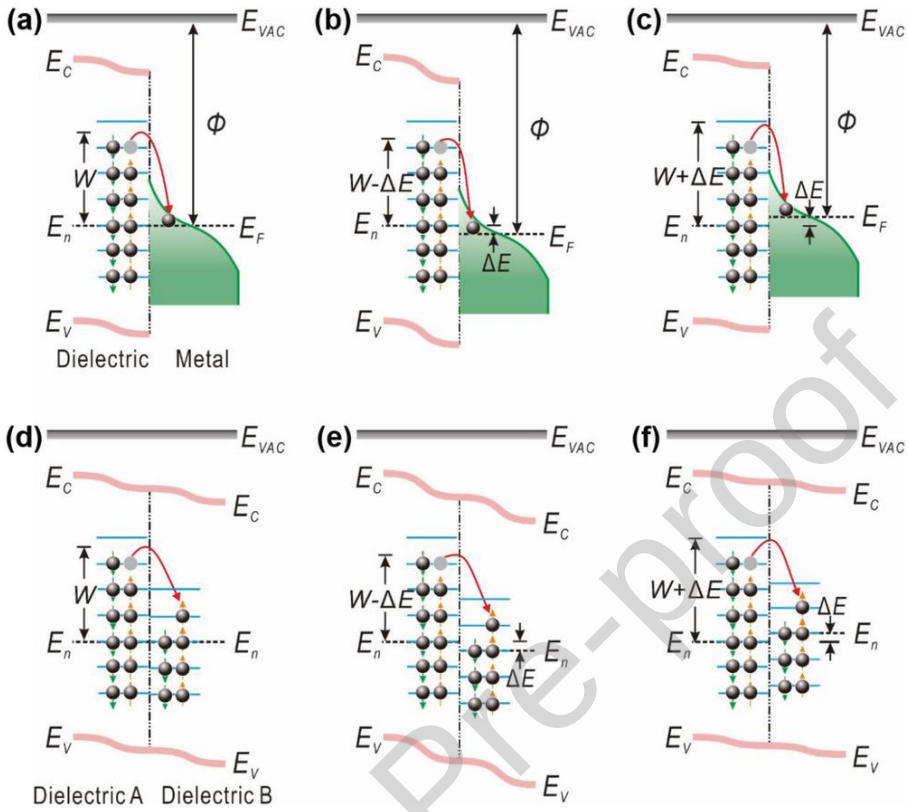

Figure13. Schematic diagram showing the basic mechanism of surface state model **Reprinted with permission** [71]. (a) Before contact of dielectric and metal, E_n and E_F lies at same level. Charge transfer between metal and dielectric when work function of metal is higher(b) and lower in (c). Before contact of two dielectrics(d) neutral level states lies at same level. Charge transfer mechanism between two dielectrics when work function of one is higher(e) and lower in(f).

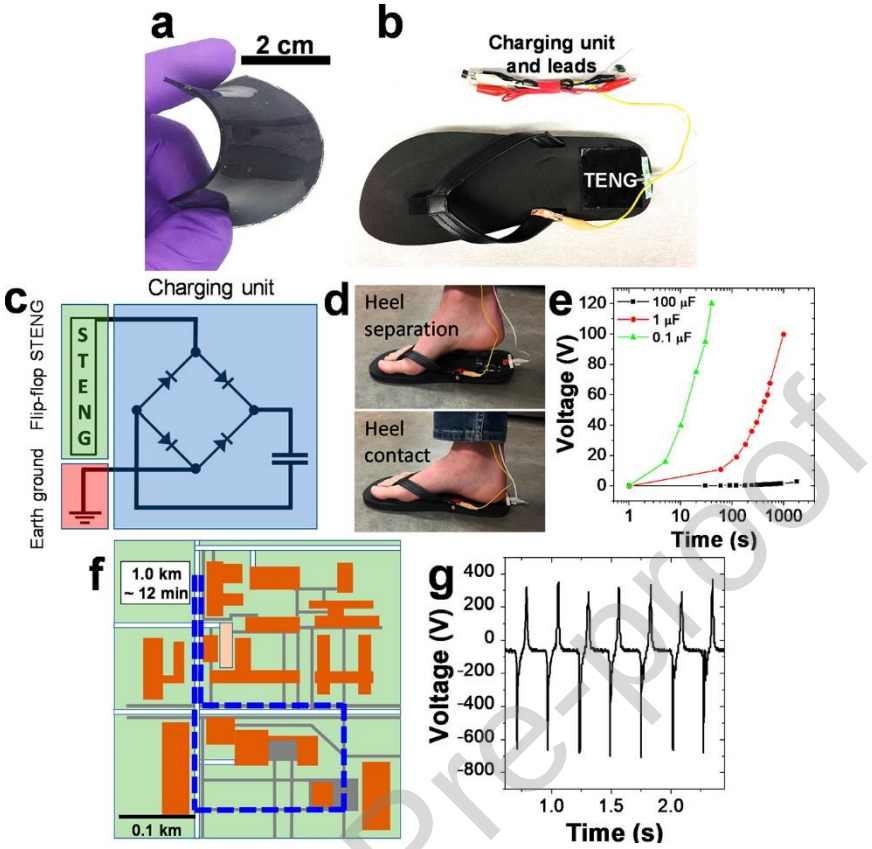

Figure 14. Output performance and circuit diagram of LIG based single electrode mode TENG **Reprinted with permission** [65] (a,b) schematic diagram of fabricated device (c) Schematic diagram of circuit of hybrid of single electrode mode TENG flip flop.(d) Seperation and contact mode of movement (e) Charging characteristics of different capacitors (f) Walking route showed by map (g) Variation of Voc with time

Credit authorship contribution statement

All authors have contributed sufficiently to the work.

Deepak Deepak: Conceptualization, Methodology, Validation, Writing – original draft, Writing – review & editing, **Navneet Soin**: Methodology, Writing – original draft, Validation, Investigation, Data curation, **Susanta Sinha Roy:** Conceptualization, Methodology, Validation, Investigation, Writing – review & editing, Supervision

Declaration of interests

☐ The authors declare that they have no known competing financial interests or personal relationships that could have appeared to influence the work reported in this paper.

☒ The authors declare the following financial interests/personal relationships which may be considered as potential competing interests:

Susanta Sinha Roy reports was provided by Shiv Nadar Institution of Eminence.